SCIENCE CHINA
Earth Sciences

• RESEARCH PAPER •

March 2014 Vol.57 No.3: 415–427
doi: 10.1007/s11430-013-4768-1

Experimental studies of melt-peridotite reactions at 1–2 GPa and 1250–1400°C and their implications for transforming the nature of lithospheric mantle and for high-Mg signatures in adakitic rocks

YU Yang[1,2], XU WenLiang[1*] & WANG ChunGuang[1]

[1] *College of Earth Sciences, Jilin University, Changchun 130061, China;*
[2] *Research Center of Palaenotology and Stratigraphy, Jilin University, Changchun 130026, China*

Received November 10, 2012; accepted April 18, 2013; published online December 3, 2013

Experiments of the melt-peridotite reaction at pressures of 1 and 2 GPa and temperatures of 1250–1400°C have been carried out to understand the nature of the peridotite xenoliths in the Mesozoic high-Mg diorites and basalts of the North China Craton, and further to elucidate the processes in which the Mesozoic lithospheric mantle in this region was transformed. We used Fuxin alkali basalt, Feixian alkali basalt, and Xu-Huai hornblende-garnet pyroxenite as starting materials for the reacting melts, and lherzolite xenoliths and synthesized harzburgite as starting materials for the lithospheric mantle. The experimental results indicate that: (1) the reactions between basaltic melts and lherzolite and harzburgite at 1–2 GPa and 1300–1400°C tended to dissolve pyroxene and precipitate low-$Mg^{\#}$ olivine ($Mg^{\#}$=83.6–89.3), forming sequences of dunite-lherzolite (D-L) and dunite-harzburgite (D-H), respectively; (2) reactions between hornblende-garnet pyroxenite and lherzolite at 1 GPa and 1250°C formed a D-H sequence, whereas reactions at 2 GPa and 1350°C formed orthopyroxenite layers and lherzolite; and (3) the reaction between a partial melt of hornblende-garnet pyroxenite and harzburgite resulted in a layer of orthopyroxenite at the boundary of the pyroxenite and harzburgite. The reacted melts have higher MgO abundances than the starting melts, demonstrating that the melt-peridotite reactions are responsible for the high-$Mg^{\#}$ signatures of andesites or adakitic rocks. Our experimental results support the proposition that the abundant peridotite and pyroxenite xenoliths in western Shandong and the southern Taihang Mountains might have experienced multiple modifications in reaction to a variety of melts. We suggest that melt-peridotite reactions played important roles in transforming the nature of the Mesozoic lithospheric mantle in the region of the North China Craton.

experimental study, melt-peridotite reaction, dunite, lithospheric mantle, North China Craton

Citation: Yu Y, Xu W L, Wang C G. 2014. Experimental studies of melt-peridotite reactions at 1–2 GPa and 1250–1400°C and their implications for transforming the nature of lithospheric mantle and for high-Mg signatures in adakitic rocks. Science China: Earth Sciences, 57: 415−427, doi: 10.1007/s11430- 013-4768-1

Unlike the Kaapvaal and Siberian cratons, the North China Craton (NCC) experienced widespread tectonothermal reactivation during the late Mesozoic and Cenozoic, and this resulted in the replacement of old, cold, thick, and depleted lithospheric mantle by young, hot, thin, and fertile mantle (Menzies et al., 1993, 1998, 2007; Griffin et al., 1998; Xu, 2001; Gao et al., 2004; Wu et al., 2005; Deng et al., 2007; Chen et al., 2008). However, the timing, extent, and mechanisms of this lithospheric thinning remain controversial. Xenoliths derived from depth are a key to reveal the nature of the NCC mantle and the ways by which the thinning proceeded.

Abundant dunite and pyroxenite xenoliths are present in Mesozoic high-Mg diorites in western Shandong, in the

*Corresponding author (email: xuwl@jlu.edu.cn)

Eastern Block of the NCC. The dunites can be subdivided into two types, based on their textures and mineral chemistry: one type has protogranular, porphyroclastic, and tabular textures, and the olivines have high $Mg^{\#}$ values (89.4–94.6); the other type displays textures typical of metamorphic deformation, the olivines have relatively low $Mg^{\#}$ values (82–87), and the rocks have undergone a later metasomatism (Xu et al., 2003, 2004). Peridotite xenoliths in the Early Cretaceous Fushan high-$Mg^{\#}$ diorites from the southern Taihang Mountains in the Trans-North China Orogen (TNCO) of the NCC are dominated by spinel harzburgites and clinopyroxene (Cpx)-poor spinel lherzolites with forsterite contents averaging 92.3, as well as minor chromite-bearing dunites with a relatively low $Mg^{\#}$ (90.1) (Xu et al., 2010). Then the questions arise: what is the origin of these dunites? Are they cumulates, or a residue formed in response to a large amount of partial melting, or are they a product of melt-peridotite reactions? Moreover, what is the origin of orthopyroxenite veining in the dunites? Previous studies on the petrogenesis of these dunites have focused mainly on petrography, mineral chemistry, and geochemistry. Although there have been some researches on melt-peridotite reactions (Fisk, 1986; Kelemen, 1990; Kelemen et al., 1990; Yaxley et al., 1998; Rapp et al., 1999; Yaxley, 2000; Morgan et al., 2005; Piccardo et al., 2007; Shaw et al., 2008; Lambart et al., 2009; Mallik et al., 2012), the experimental studies that can be applied to the above questions are few and far between (Wang et al., 2010; Zhang et al., 2012).

In this paper, we describe a series of high-pressure and high-temperature (HP-HT) experiments using various basalts and pyroxenites for the reacting melts, and lherzolites and harzburgites as representatives of the mantle peridotites. We focused on the lithological and compositional changes in both the peridotites and the melts to better understand: (1) the petrogenesis of different types of peridotite xenoliths; (2) the nature of the changes in the Mesozoic lithospheric mantle beneath the NCC; and (3) the petrological implications for the high-Mg signatures of adakitic rocks.

1 Materials and methods

1.1 Starting materials

The starting materials for the reacting melts were powdered natural alkali basalts (FW1-1, FX-1) and hornblende-garnet (Hb-Grt) pyroxenite (JG4-1). The basalts were collected from Fuxin in Liaoning Province (Zheng et al., 1999) and Feixian in western Shandong Province (Pei et al., 2004), and the pyroxenite came from the Jiagou adakitic intrusion in Anhui Province (Xu et al., 2009). According to the literature, the Fuxin and Feixian alkali basalts were derived from asthenospheric mantle (Zheng et al., 1999; Wang, 2002) and lithospheric mantle (Pei et al., 2004), respectively, whereas the Hb-Grt pyroxenite can be attributed to the NCC basement (Xu et al., 2009). A natural lherzolite powder (WFY-1) and a synthesized harzburgite powder (WFY-2) represent mantle peridotites. Sample WFY-1 is a peridotite xenolith from the Cenozoic basalts of Huinan, Jilin Province, and it consists of 52.9 wt.% olivine, 32.6 wt.% orthopyroxene (Opx), 13.1 wt.% Cpx, and 1.4 wt.% spinel, according to the MINSQ method (Herrmann et al., 2002). Sample WFY-2 was synthesized by mixing crushed, optically clean olivine (50 wt.%) and Opx (50 wt.%), collected from sample WFY-1. Compositions of the starting materials are listed in Table 1.

FW1-1: an alkali basalt from Fuxin in Liaoning Province;

Table 1 Starting compositions of whole rocks and minerals (wt.%)

	FW1-1	FX-1	JG4-1	WFY-1	WFY-2	WFY-1			
						Ol	Opx	Cpx	Sp
SiO_2	44.28	48.77	46.27	45.77	47.19	39.99	54.38	51.42	0.09
TiO_2	2.82	1.09	1.68	0.11	0.05	0.00	0.10	0.41	0.12
Al_2O_3	14.30	11.71	11.46	3.17	2.18	0.04	4.31	6.01	55.88
Cr_2O_3					0.19	0.03	0.35	0.71	11.21
Fe_2O_3	12.96	8.09	19.75	8.59					
FeO					8.07	10.00	6.13	2.87	11.16
MnO	0.19	0.12	0.25	0.12	0.12	0.06	0.17	0.13	0.08
MgO	8.55	13.59	8.12	38.27	39.98	47.66	32.30	15.54	20.64
CaO	10.50	8.82	11.41	3.09	0.42	0.07	0.76	20.12	0.00
Na_2O	2.70	2.22	0.46	0.31	0.07	0.01	0.13	1.51	0.05
K_2O	2.13	2.38	0.04	<0.01	0.01	0.01	0.00	0.00	0.02
P_2O_5	0.05	0.66	0.04	0.01					
NiO					0.24	0.39	0.08	0.00	0.37
LOI	1.50	1.33	0.16	-0.31					
Total	99.11	98.78	99.64	99.13	98.49	98.26	98.71	98.72	99.62
$Mg^{\#}$	56.7	76.9	44.9	89.8	89.9	89.5	90.4	90.6	76.8
$Cr^{\#}$									11.9

FX-1: an alkali basalt from Feixian in western Shandong Province; JG4-1: a Hb-Grt pyroxenite xenolith from Jiagou intrusion in northern Anhui Province; WFY-1: a lherzolite xenolith from Huinan in Jilin Province; WFY-2: a synthetic harzburgite, and its compositions produced by mixing olivine and orthopyroxene collected from WFY-1 in weight proportions of 0.5∶0.5; Cpx-clinopyroxene; Ol-olivine; Opx-orthopyroxene; Sp-spinel. LOI: loss on ignition; $Mg^{\#}$=molar 100 Mg/(Mg+Fe); $Cr^{\#}$=molar 100 Cr/(Cr+Al).

1.2 Experimental methods

To simulate the reaction between melt and peridotite at depths of the lithospheric mantle, a series of HP-HT experiments were carried out at pressures of 1 or 2 GPa and temperatures of 1250–1400°C, with the positions of the solidus and liquidus for fertile peridotites and basalts taken into account (Figure 1). All the experiments were conducted in a non-end-loaded type piston-cylinder (Quickpress 3.0) at the State Key Laboratory of Geological Processes and Mineral Resources of China University of Geoscience.

As shown in Figure 2, the furnace assembly consists of a Pt capsule, placed in a thin-walled BN sleeve, and then sandwiched between two crushable MgO spacer rods in another sleeve of graphite, Pyrex® and salt. The experimental samples were made up of a layer of basalt or pyroxenite on top of a layer of peridotite, and they were packed in the graphite-lined Pt capsule (5.7 mm high and 5 mm outer diameter for the Pt capsule, 4.3 mm outer diameter and 2.2 mm inner diameter for the graphite tube) in order to prevent Fe loss. Prior to sealing the Pt tube, the open capsule and furnace assembly were stored in a vacuum oven at 110°C for at least 12 hours. A W_5Re_{95}-$W_{26}Re_{74}$ thermocouple, situated at the bottom of the sample capsule, was used to continually monitor temperatures during the experiment. For these experiments, temperature and pressure errors are expected to be less than 10°C and 0.1 GPa, respectively, based on previous calibrations (Wang et al., 2010).

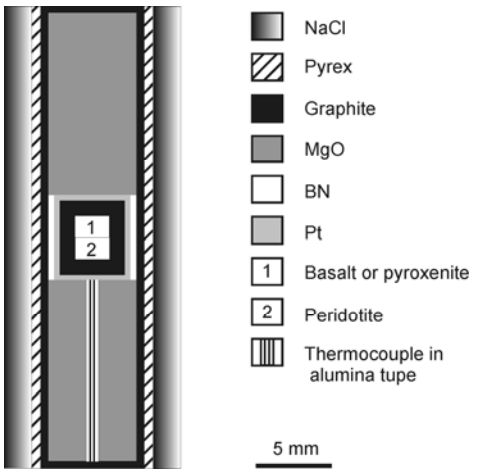

Figure 2 Piston-cylinder assembly.

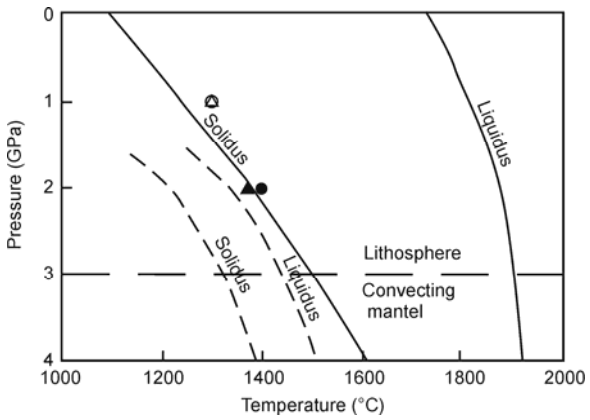

Figure 1 *P-T* plot showing solidus and liquidus for fertile peridotite (solid curve) and average MORB (dashed curve). A representative thickness for the continental lithosphere is shown as the horizontal dashed line (after Yaxley (2000)). The filled circle, open circle, filled triangle, and open triangle represent run FW0912, FH0629, FXH0704, and FXH0703, respectively.

The charge was first cold pressurized to run pressure changes at a rate of 7 MPa/min, and then the conditions were held at the desired pressure for several hours. The temperatures were programmed to move towards the desired temperature at a rate of 10°C/min. Once the desired conditions of *T* and *P* were reached, the sample was kept at that *T* and *P* for a number of hours. The samples were then decompressed at a rate of 4 MPa/min, and quenched to below 200°C within 10 s by turning off the power of the press. The recovered Pt capsules were sectioned perpendicular to the cylindrical axis using a low-speed diamond saw, mounted in epoxy, and polished for microprobe analysis. Table 2

Table 2 Run conditions for all experiments and phase assemblage of the reactive sample[a)]

Run number	Starting material	Pressure (GPa)	Temperature (°C)	Duration	Phase assemblage (in peridotite)
FW0912	FW1-1+WFY-1	2	1400	8	Duntie (glass+Ol)+Lher. (Ol+Opx+Cpx)
FH0629	FW1-1+WFY-2	1	1300	8	Dunite (glass+Ol)+Harz. (Ol+Opx)
FXH0703	FX-1+WFY-2	1	1300	8	Dunite (glass+Ol)+Harz. (Ol+Opx)
FXH0704	FX-1+WFY-2	2	1370	8	Dunite (glass+Ol)+Harz. (Ol+Opx)
JW1011	JG4-1+WFY-1	1	1250	24	Dunite (glass+Ol)+Harz. (glass+Ol+Opx)
JW0912	JG4-1+WFY-1	2	1350	10	Opx+Lher. (Ol+Opx+Cpx)
JH0627	JG4-1+WFY-2	2	1300	24	Opx+Harz. (Ol+Opx)

a) Harz.-harzburgite; Lher.-lherzolite.

summarizes the experimental conditions.

1.3 Analytical methods

Whole rock major element data were obtained by X-ray fluorescence (XRF) using a Rigaku RIX 2100 spectrometer at the State Key Laboratory of Continental Dynamics, Northwest University, China. The major element compositions of minerals, starting material melts, and experimental samples were determined using a JEOL JXA-8100 electron microprobe at the Key Laboratory of Orogenic Belts and Crustal Evolution, Peking University, China. The analytical conditions were an accelerating voltage of 15 kV, a beam current of 20 nA, and a beam diameter of 1 μm for minerals. For melt analyses, Na and K were analyzed first, and the beam diameter was 5 μm.

2 Results

2.1 Phase assemblages

A zone of dunite was formed in all the basalt-peridotite reaction experiments at 1–2 GPa and 1300–1400°C (Figure 3(a)–(d)). The alkali basalts (FW1-1, FX-1) were totally melted whereas neither lherzolite nor harzburgite was melted. Reaction between basaltic melt and the underlying peridotite caused the Opx to be dissolved in the basaltic melt, and a zone of dunite with an interstitial melt was formed. The reaction zone that formed at 1 GPa and 1300°C (Figure 3(b), (c)) is much wider than that formed at 2 GPa and 1400/1370°C (Figure 3(a), (d)) over the same length of time. The interface is quite distinct between the regions of dunite and harzburgite.

In the pyroxenite-peridotite experiments at 1 GPa (JW1011) and 1250°C, the Hb-Grt pyroxenite (JG4-1) became totally molten near the melt-peridotite boundary, but some recrystallized Opx appeared at the top of the sample capsule (Figure 3(e)). Dissolution of lherzolite in the melt resulted in a sequence of dunite-harzburgite (D-H). In the pyroxenite-peridotite experiments at 2 GPa and 1350°C (JW0912), the Hb-Grt pyroxenite was totally melted, but only a small amount of melt appeared at the hot end (geometric "top") of the capsule. A thin layer of Opx was formed adjacent to the peridotite. Meanwhile, a number of amphibole crystals were precipitated next to the Opx layer (Figure 3(f)). This is similar to the results of some other amphibole-forming experiments (Sen et al., 1994), but different from our experimental results at 1 GPa.

In the pyroxenite-peridotite experiment at 2 GPa and 1300°C (JH0627), the Hb-Grt pyroxenite was partially melted leaving a residue of garnets, and the reaction between the harzburgite and the partial melt (SiO_2=48.82 wt.%–51.03 wt.%) of Hb-Grt pyroxenite produced a layer of orthopyroxenite at the melt-peridotite interface.

2.2 Melt compositions

Comparing the reacted melt with the starting melt is useful when assessing the effect of peridotite assimilation on the compositional variation of the melts. Compositions of reacted melts in runs FW0912, FH0629, FXH0703, FXH0704 and JW1011 are listed in Table 3. The melt composition in run JW1011 has been corrected by adding the appropriate amount of crystalline Opx back into the bulk melt. Within the dunites, the calculated FeO/MgO olivine-melt partition coefficients are 0.31 in run FW0912, 0.16–0.27 in run FH0629, 0.17–0.27 in run FXH0703, 0.16–0.20 in run FXH0704, and 0.33 in run JW1011. Based on the partition coefficient for olivine-melt equilibrium (0.30±0.03) (Roeder et al., 1970), it is suggested that the reacting melts and olivines are not in equilibrium except in runs FW0912 and JW1011.

Figure 4 shows the melt composition profiles in the region from alkali basalt or pyroxenite (x>0) to peridotite (x< 0). In the experiments on the reaction between Fuxin alkali basalt and peridotite (runs FW0912 and FH0629), (1) SiO_2 and MgO contents increase in the reacted melts while FeO decreases; (2) Al_2O_3 increases in the interstitial melts (x<0) at high pressure, but decreases at low pressure; (3) CaO in the melts increases towards the basalt-dunite interface (x=0), whereas MgO sharply decreases in the interstitial melts; and (4) Na_2O and K_2O contents increase slightly towards the basalt-dunite interface (Figure 4).

In the experiments on the reaction between Feixian alkali basalt and peridotite (runs FXH0703 and FXH0704), the compositional variations of the melts are similar to those in the experiments on Fuxin alkali basalt and peridotite (Figure 4). But, the reacted melts in runs FXH0703 and FXH0704 have lower MgO and higher FeO than their starting melts, which is the opposite of the experimental results in runs FW0912 and FH0629 (Figure 4(b), (c)). This is because sample FX-1 has a higher MgO and lower FeO than sample FW1-1.

In the pyroxenite-peridotite reaction experiment (run JW1011), the trend of compositional variations in the melts is more continuous than in the reactions referred to above (Figure 4), suggesting a relative state of equilibrium. Compared with the starting melts, the reacted melts have higher contents of SiO_2 and MgO, lower Al_2O_3, FeO, and CaO, and slightly higher Na_2O.

2.3 Mineral compositions

The major element compositions of representative minerals in these experiments are listed in Table 4. Newly developed olivine can be observed in the dunite zone. As shown in Figure 5, individual olivine grains reflect the core-to-rim variations in runs FW0912 and JW0912 (Figure 5(a)–(d)). The olivine cores, compared to their rims, have a higher $Mg^{\#}$ and NiO content, but a lower FeO and CaO. Compositional

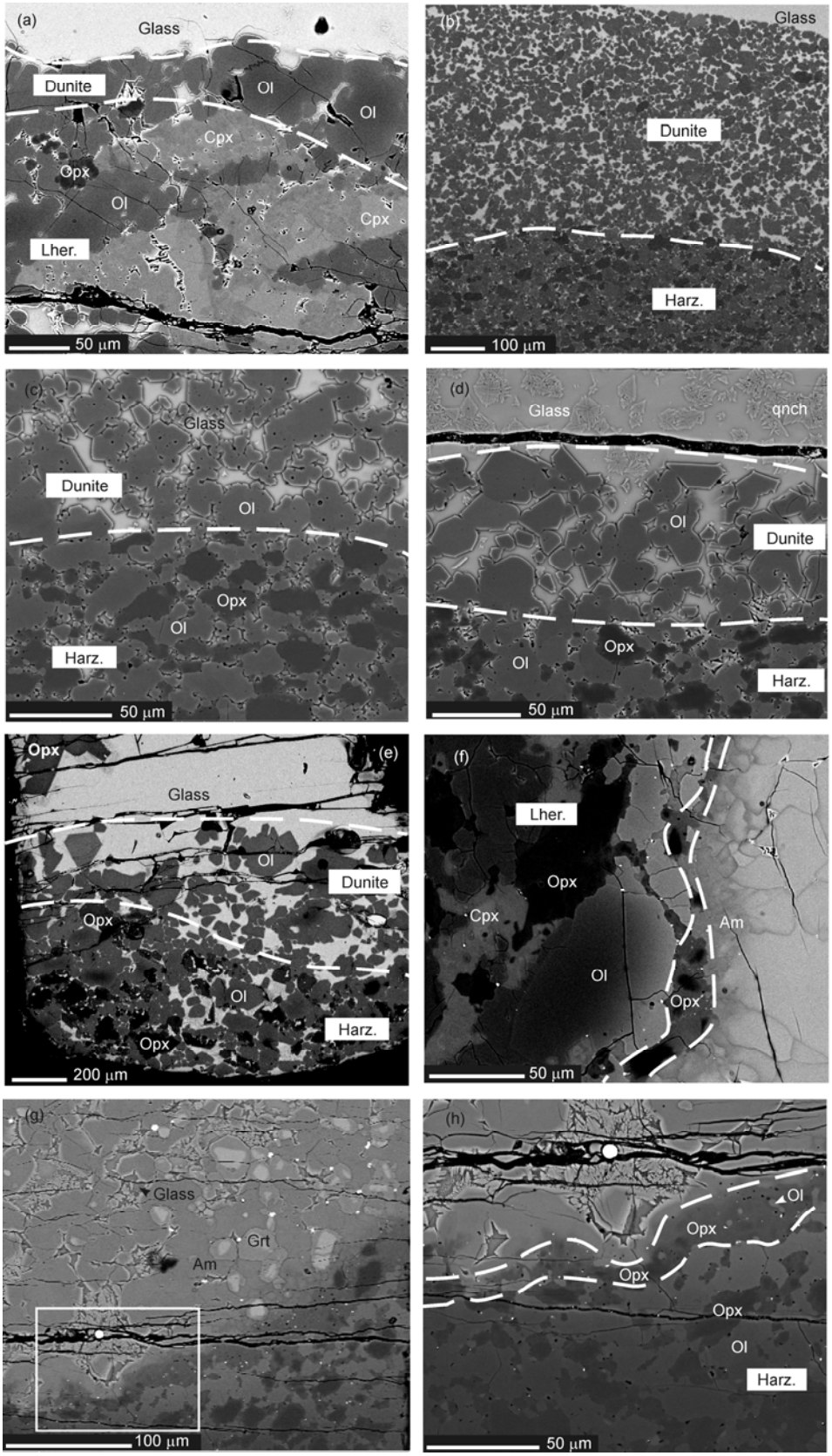

Figure 3 Back-scattered electron (BSE) photomicrographs of crystal-melt phase assemblages in melt-peridotite layered experiments at 1 and 2 GPa. Dashed curves mark the melt-peridotite contact and sharp lithological boundaries. Olivine, orthopyroxene, and clinopyroxene are shown as medium gray, dark gray, and light gray in the BSE images of peridotite, respectively. (a) Run FW0912; (b) run FH0629; (c) run FXH0703; (d) run FXH0704; (e) run JW1011; (f) run JW0912; (g) an overall view of run JH0627; (h) close-up view of the melt-peridotite contact in run JH0627.

Table 3 Compositions of reacted melts in runs FW0912, FH0629, FXH0703, FXH0704 and JW1011 (wt.%)

Sample	FW0912											
Phase	glass	glass	glass	glass	glass	glass	glass	glass	glass	glass	crystal	crystal
SiO_2	44.64	44.69	44.03	44.38	45.10	44.79	44.29	44.98	44.67	45.07	46.35	46.13
TiO_2	2.71	2.68	2.68	2.83	2.84	2.91	2.90	2.92	2.81	2.71	3.16	2.95
Al_2O_3	14.78	14.67	14.44	14.83	15.04	14.91	14.82	14.90	14.80	14.54	16.65	17.03
Cr_2O_3	0.05	0.03	0.06	0.07	0.02	0.08	0.04	0.03	0.00	0.06	0.11	0.09
FeO	10.29	10.14	10.69	10.43	10.37	10.44	10.50	10.31	10.58	10.41	9.63	9.42
MnO	0.20	0.24	0.14	0.13	0.15	0.18	0.18	0.17	0.22	0.19	0.17	0.14
MgO	11.34	11.22	11.25	11.21	11.21	11.46	11.54	12.28	11.63	11.57	5.51	5.08
CaO	8.44	8.65	8.31	8.48	8.45	8.45	8.45	8.46	8.49	8.58	10.02	8.94
Na_2O	2.69	2.82	2.82	2.71	2.80	2.66	2.69	2.39	2.87	2.56	2.43	2.51
K_2O	1.86	2.09	2.02	2.12	1.91	1.94	1.97	1.99	1.91	1.83	2.32	2.58
NiO	0.01	0.03	0.01	0.06	0.04	0.00	0.00	0.05	0.00	0.00	0.07	0.05
Total	97.01	97.26	96.45	97.25	97.93	97.82	97.38	98.47	97.98	97.52	96.42	94.92
$Mg^{\#}$	66.3	66.4	65.3	65.8	65.9	66.2	66.3	68.0	66.3	66.5	50.5	49.1
Sample	FH0629										FXH0703	
Phase	glass	glass	glass	glass	glass	crystal	crystal	crystal	crystal	crystal	glass	glass
SiO_2	45.56	45.33	45.54	46.43	47.15	48.09	49.91	50.02	50.83	52.44	47.08	46.29
TiO_2	2.41	2.33	2.35	2.33	2.45	2.83	2.27	1.86	1.73	1.40	2.70	2.51
Al_2O_3	13.82	14.13	13.61	13.21	13.42	15.27	14.36	12.96	12.48	11.94	14.64	14.46
Cr_2O_3	0.14	0.07	0.06	0.12	0.14	0.12	0.01	0.09	0.05	0.07	0.02	0.04
FeO	9.78	9.72	9.58	9.65	10.23	9.07	8.79	9.50	9.27	9.02	9.77	9.59
MnO	0.19	0.16	0.23	0.19	0.20	0.12	0.18	0.19	0.22	0.19	0.18	0.19
MgO	12.49	12.18	12.42	12.95	11.22	6.50	6.70	9.21	8.72	8.95	11.01	10.69
CaO	8.79	8.93	8.61	8.58	9.49	10.02	10.39	9.56	9.65	9.38	8.70	8.76
Na_2O	2.49	2.54	2.46	2.45	2.74	2.86	2.84	2.80	2.85	3.21	3.04	2.96
K_2O	1.71	1.76	1.70	1.61	1.43	1.85	1.93	1.72	1.75	1.89	1.76	1.70
NiO	0.00	0.00	0.00	0.00	0.00	0.02	0.03	0.03	0.02	0.14	0.09	0.06
Total	97.38	97.15	96.56	97.52	98.47	96.75	97.41	97.95	97.58	98.63	98.99	97.25
$Mg^{\#}$	69.5	69.1	69.8	70.6	66.2	56.1	57.7	63.4	62.7	63.9	66.8	66.6
Sample	FXH0703									FXH0704		
Phase	glass	glass	glass	crystal	crystal	crystal	crystal	crystal	crystal	glass	glass	glass
SiO_2	46.30	47.32	47.77	48.04	51.52	49.55	50.86	51.86	52.94	45.28	45.48	45.97
TiO_2	2.84	2.35	2.39	3.01	1.80	2.39	2.20	1.85	1.71	3.18	3.32	3.24
Al_2O_3	14.52	13.69	14.22	15.08	15.18	14.05	13.54	13.39	14.50	15.39	14.81	15.55
Cr_2O_3	0.07	0.10	0.09	0.06	0.11	0.10	0.06	0.07	0.10	0.02	0.03	0.04
FeO	9.71	9.67	10.15	9.08	8.58	9.09	9.04	8.62	7.47	10.24	9.97	9.08
MnO	0.18	0.18	0.17	0.18	0.19	0.21	0.20	0.19	0.19	0.15	0.15	0.14
MgO	10.80	11.04	10.16	7.43	6.42	7.80	7.61	7.68	5.92	10.42	10.91	9.25
CaO	8.91	8.82	9.19	9.75	9.95	9.99	9.75	9.05	9.22	7.74	7.44	8.51
Na_2O	2.93	2.85	3.22	3.22	3.09	3.20	3.43	3.44	3.76	3.62	3.26	3.70
K_2O	1.55	1.57	1.65	1.75	2.01	1.64	1.82	2.18	2.42	2.15	2.27	2.07
NiO	0.01	0.00	0.10	0.00	0.02	0.09	0.00	0.04	0.02	0.00	0.04	0.00
Total	97.82	97.59	99.10	97.61	98.86	98.10	98.51	98.37	98.26	98.20	97.67	97.55
$Mg^{\#}$	66.5	67.1	64.1	59.4	57.2	60.5	60.1	61.4	58.6	64.5	66.2	64.5
Sample	FXH0704			JW1011								
Phase	crystal	crystal	crystal	glass	glass	glass	glass	glass	crystal	crystal	crystal	
SiO_2	46.19	47.11	47.60	47.59	47.46	47.20	47.63	47.52	47.51	47.10	48.08	
TiO_2	3.55	3.49	3.87	1.15	1.19	1.18	1.11	1.14	1.18	1.18	1.16	
Al_2O_3	16.72	17.26	17.62	10.16	10.25	10.22	10.27	10.46	10.17	10.34	10.26	
Cr_2O_3	0.00	0.05	0.02	0.17	0.23	0.17	0.14	0.14	0.13	0.18	0.24	
FeO	9.39	8.91	8.45	13.45	13.13	13.05	13.18	12.98	12.84	13.24	13.14	
MnO	0.21	0.17	0.15	0.24	0.22	0.23	0.21	0.22	0.22	0.24	0.22	
MgO	6.55	5.48	4.48	14.69	14.72	14.50	14.66	14.70	13.96	14.09	14.10	
CaO	9.11	9.28	9.68	10.65	10.58	10.67	10.59	10.56	10.50	10.66	10.41	
Na_2O	3.37	3.54	3.49	0.60	0.60	0.63	0.63	0.63	0.63	0.61	0.56	
K_2O	2.20	2.18	2.47	0.05	0.05	0.05	0.05	0.03	0.02	0.02	0.05	
NiO	0.00	0.00	0.00	0.05	0.00	0.07	0.00	0.00	0.02	0.02	0.02	
Total	97.29	97.47	97.82	98.78	98.42	97.96	98.45	98.37	97.17	97.68	98.24	
$Mg^{\#}$	55.5	52.4	48.6	66.1	66.7	66.5	66.5	66.9	66.0	65.5	65.7	

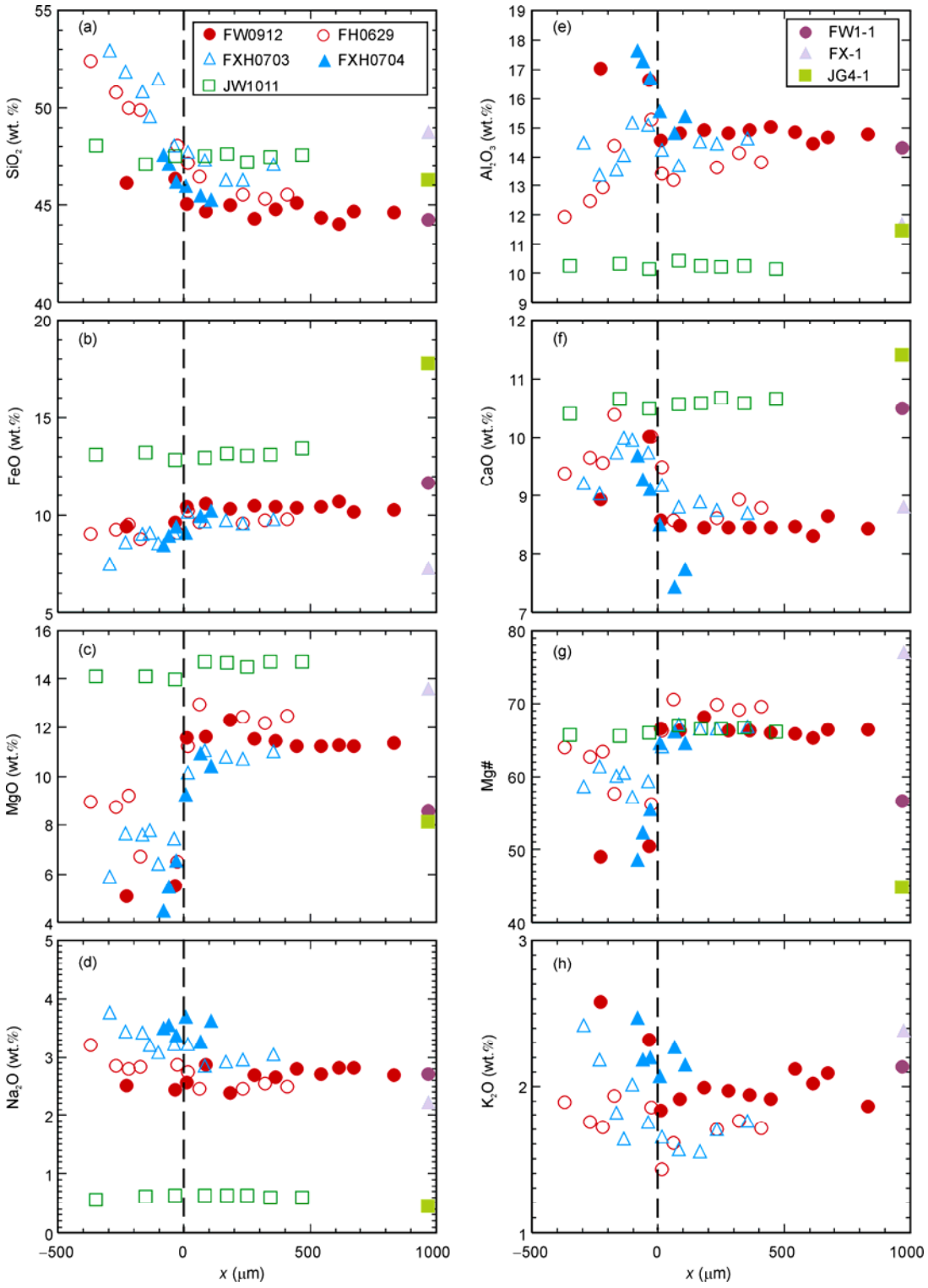

Figure 4 Plots of measured oxide abundance (in wt.%) in melt as a function of distance (x) in melt-peridotite layered experiments. The melt-peridotite interface is at x=0. The glass phase is at x>0, and the crystal phase is at x<0.

variations in olivines as a function of distance (x) are also shown in Figure 5(e)–(h). From the melt-dunite interface to the harzburgite, the $Mg^{\#}$ of olivines increases from 88.0 to 89.8 in run FH0629, from 86.8 to 89.8 in run FXH0703, from 86.0 to 87.3 in run FXH0704, and from 83.6 to 85.6 in run JW1011. Similarly, in these runs, the FeO and CaO contents of the olivines decrease, and NiO increases from the melt-dunite interface to the harzburgite.

Table 4 Representative mineral compositions in melt-peridotite layered experiments (wt.%)[a)]

Sample	FW0912		FH0629				FXH0703			
	Ol-c dunite	Ol-r dunite	Ol2 dunite	Ol9 dunite	Ol10 dunite	Ol12 Harz.	Ol1 dunite	Ol5 dunite	Ol7 dunite	Ol10 Harz.
SiO_2	40.37	40.24	40.76	40.27	40.07	40.42	40.75	40.59	40.27	40.68
TiO_2	0.00	0.05	0.06	0.02	0.00	0.01	0.04	0.02	0.00	0.04
Al_2O_3	0.04	0.11	0.05	0.07	0.04	0.07	0.05	0.00	0.00	0.05
Cr_2O_3	0.06	0.02	0.09	0.10	0.08	0.08	0.08	0.11	0.05	0.03
FeO	10.59	13.00	11.30	11.15	10.71	10.04	12.68	12.01	11.69	10.43
MnO	0.13	0.13	0.19	0.18	0.13	0.11	0.23	0.20	0.20	0.15
MgO	48.27	47.33	47.24	47.56	47.88	47.59	46.92	47.22	46.74	48.58
CaO	0.14	0.21	0.22	0.21	0.27	0.17	0.22	0.19	0.17	0.13
Na_2O	0.00	0.00	0.00	0.03	0.03	0.01	0.02	0.02	0.02	0.02
K_2O	0.00	0.00	0.00	0.01	0.00	0.00	0.00	0.00	0.01	0.00
NiO	0.36	0.27	0.16	0.11	0.20	0.18	0.09	0.18	0.09	0.23
Total	99.96	101.35	100.06	99.71	99.42	98.68	101.08	100.54	99.24	100.34
$Mg^{\#}$	89.1	86.7	88.2	88.4	88.9	89.4	86.9	87.5	87.7	89.3

Sample	FXH0704				JW1011				JW0912	
	Ol1 dunite	Ol5 dunite	Ol7 Harz.	Ol9 Harz.	Ol24 dunite	Ol19-c dunite	Ol18-r dunite	Ol15 Harz.	Ol-r Lherz.	Ol-c Lherz.
SiO_2	40.21	40.13	40.07	39.80	38.26	39.29	38.77	38.63	37.69	39.61
TiO_2	0.14	0.08	0.04	0.01	0.00	0.00	0.03	0.00	0.06	0.00
Al_2O_3	0.14	0.11	0.09	0.09	0.07	0.04	0.05	0.10	0.11	0.08
Cr_2O_3	0.03	0.02	0.00	0.04	0.10	0.03	0.10	0.15	0.01	0.04
FeO	13.34	13.60	12.27	12.07	15.75	12.28	15.25	15.03	19.09	11.15
MnO	0.16	0.15	0.18	0.13	0.19	0.16	0.25	0.16	0.22	0.13
MgO	45.82	45.93	45.93	46.34	44.81	48.14	45.77	45.13	41.44	47.54
CaO	0.29	0.28	0.20	0.22	0.32	0.11	0.35	0.32	0.31	0.21
Na_2O	0.05	0.01	0.04	0.01	0.00	0.00	0.01	0.00	0.01	0.01
K_2O	0.04	0.00	0.00	0.00	0.00	0.00	0.00	0.00	0.01	0.00
NiO	0.02	0.05	0.23	0.27	0.05	0.19	0.07	0.03	0.15	0.36
Total	100.24	100.35	99.04	98.98	99.55	100.24	100.65	99.55	99.12	99.13
$Mg^{\#}$	86.0	85.8	87.0	87.3	83.6	87.5	84.3	84.3	79.5	88.4

Sample	FW0912		FH0629			FXH0703				
	Opx4.1 Lherz.	Opx7.1 Lherz.	Opx3-c Harz.	Opx2-r Harz.	Opx5 Harz.	Opx1 Harz.	Opx2-c Harz.	Opx3-r Harz.	Opx4-c Harz.	Opx5-r Harz.
SiO_2	54.61	54.16	53.92	54.29	54.37	55.49	54.51	55.18	54.77	55.13
TiO_2	0.09	0.08	0.13	0.10	0.07	0.11	0.04	0.08	0.09	0.07
Al_2O_3	4.46	4.50	4.70	4.08	4.40	4.09	4.90	4.26	4.55	4.20
Cr_2O_3	0.35	0.42	0.33	0.33	0.27	0.33	0.34	0.39	0.39	0.42
FeO	6.75	6.64	6.61	6.28	6.39	6.58	6.26	6.63	6.26	6.35
MnO	0.19	0.07	0.14	0.09	0.12	0.14	0.17	0.15	0.12	0.12
MgO	32.08	32.11	32.71	32.99	33.15	32.09	32.45	32.69	32.85	32.87
CaO	0.79	0.78	0.75	0.75	0.52	0.59	0.68	0.78	0.47	0.53
Na_2O	0.09	0.16	0.07	0.11	0.03	0.05	0.09	0.09	0.11	0.08
K_2O	0.00	0.00	0.01	0.01	0.02	0.01	0.00	0.02	0.00	0.00
NiO	0.15	0.11	0.09	0.04	0.07	0.14	0.16	0.08	0.13	0.05
Total	99.56	99.03	99.46	99.07	99.40	99.62	99.60	100.34	99.74	99.82
$Mg^{\#}$	89.5	89.6	89.8	90.4	90.3	89.7	90.3	89.8	90.4	90.2

Sample	FXH0704				JW1011			
	Opx2-c Harz.	Opx1-r Harz.	Opx4-c Harz.	Opx3-r Harz.	Opx3-c Harz.	Opx4-r Harz.	Opx6-c Harz.	Opx7-r Harz.
SiO_2	54.04	53.33	54.21	54.24	53.53	53.42	53.80	54.98
TiO_2	0.11	0.29	0.07	0.19	0.11	0.16	0.14	0.13
Al_2O_3	4.22	5.03	4.29	4.46	4.66	3.00	4.41	1.72
Cr_2O_3	0.23	0.38	0.37	0.36	0.36	0.66	0.21	0.27
FeO	6.62	7.08	6.26	6.92	6.35	8.57	6.64	8.66
MnO	0.13	0.14	0.13	0.15	0.14	0.20	0.11	0.15
MgO	33.14	30.81	32.57	31.46	33.39	30.58	34.08	31.03
CaO	0.73	1.52	0.78	1.12	0.74	2.45	0.89	2.18
Na_2O	0.10	0.22	0.11	0.21	0.00	0.03	0.02	0.03
K_2O	0.00	0.00	0.02	0.02	0.00	0.00	0.00	0.00
NiO	0.02	0.09	0.05	0.10	0.07	0.02	0.07	0.03
Total	99.34	98.88	98.85	99.22	99.35	99.09	100.36	99.17
$Mg^{\#}$	89.9	88.6	90.3	89.0	90.4	86.4	90.2	86.5

(*To be continued on the next page*)

(*Continued*)

Sample	JW0912		JH0627					
	Opx-c Opx zone	Opx-r Opx zone	Opx1-c Opx zone	Opx3-r Opx zone	Opx5-c Opx zone	Opx6-r Opx zone	Opx12-c Harz.	Opx13-r Harz.
SiO_2	52.90	49.31	55.12	51.24	54.43	50.59	55.22	52.99
TiO_2	0.08	0.28	0.07	0.77	0.09	0.74	0.11	0.47
Al_2O_3	4.55	7.76	4.56	8.08	5.00	8.07	5.06	6.92
Cr_2O_3	0.37	0.26	0.31	0.18	0.38	0.24	0.35	0.35
FeO	8.04	10.55	6.38	11.51	6.31	11.08	6.54	6.93
MnO	0.15	0.18	0.17	0.24	0.18	0.13	0.17	0.19
MgO	31.36	26.27	32.78	27.03	32.11	26.59	32.57	30.50
CaO	0.95	2.11	0.83	1.63	0.97	1.61	0.98	1.58
Na_2O	0.06	0.10	0.09	0.05	0.12	0.12	0.09	0.12
K_2O	0.00	0.00	0.00	0.02	0.00	0.01	0.01	0.02
NiO	0.09	0.02	0.17	0.06	0.14	0.06	0.12	0.08
Total	98.54	96.84	100.47	100.80	99.73	99.24	101.21	100.14
$Mg^{\#}$	87.5	81.6	90.2	80.8	90.1	81.1	89.9	88.7

a) c-core; r-rim.

In the basalt-peridotite and pyroxenite-peridotite reaction experiments at 1 GPa, Opx is originally present in the lherzolite or harzburgite zone. The core-to-rim compositional variations of these Opx can be observed in the harzburgite zone in runs FXH0704 and JW1011. The rims of the Opx have higher FeO and CaO but lower MgO than the cores. Newly developed Opx is present as a thin layer in the reaction zone in the pyroxenite-peridotite experiment at 2 GPa, and also present in the partial melt during the pyroxenite-peridotite experiments (runs JW0912 and JH0627). The newly developed Opx with neoblasts precipitated on the surface of the original Opx in the reaction zone shows clear compositional variations from core to rim. The cores have the same compositional characteristics as Opx originally present in the samples, but the rims have higher Al_2O_3, FeO, and CaO contents, and lower SiO_2 and MgO (Table 4).

3 Discussions

3.1 Sequence of lithological changes: Implications for changes in the nature of lithospheric mantle

The reactions between peridotite and different types of melt result not only in a sequence of lithological changes, but also changes in the compositions of minerals and melts. Preferential dissolution of Cpx and Opx, as well as precipitation of olivine, gives rise to the formation of dunite, whereas precipitation of Opx creates a layer of orthopyroxenite in runs JW0912 and JH0627. Whether it is olivine or Opx that is consumed during the melt-peridotite reaction depends mainly on the nature of the reacting melts, and in particular, whether the melts are close to olivine or Opx saturation (Morgan et al., 2005). Variations in the compositions of olivine and Opx during each sequence of lithological change are controlled by the reacting melt and the host minerals. The core-to-rim compositional variations of newly developed olivine and Opx in the reaction zone are controlled by the reaction between the original peridotite and the reacting melts, and the variations can be attributed to the gradually evolving nature of the reacting melt.

Although a similar initial material (i.e., JG4-1) was used in runs JW1011 (at 1 GPa and 1250°C) and JW0912 (at 2 GPa and 1350°C), the products are different: run JW1011 produced olivine, whereas run JW0912 produced Opx, and this may have been a result of the different pressures. The absence of Opx at the melt-peridotite interface in run JW1011 could be ascribed to the incongruent melting of Opx at low pressures (Opx→olivine+Si-rich melt) (Kubo, 2002).

Melt compositions in these experiments are controlled by pyroxene dissolution, olivine precipitation, and diffusive exchange (Morgan et al., 2005). In runs FW0912, FH0629, and JW1011, because Opx and Cpx have higher SiO_2 and MgO than the pristine melt (Table 1), dissolution of the Opx and Cpx will increase the amounts of SiO_2 and MgO in the hybridized melts (Figure 4(a), (c)). On the other hand, the dissolution had a dilution effect with regard to the amounts of Al_2O_3, FeO, and CaO in the hybridized melts (Figure 5(b), (e), (f)). The sharp decline in MgO (Figure 4(c)) and the rise in CaO (Figure 4(f)) in interstitial melts may be a consequence of the precipitation of olivine.

Kelemen et al. (1998) described the reaction types as:

$$\text{Olivine}+SiO_2(\text{melt}_1)=\text{Opx}(+\text{melt}_2) \quad (1)$$

$$\text{Opx}+\text{melt}_1=\text{olivine}+SiO_2(\text{melt}_2) \quad (2)$$

Reaction (1) is likely to occur where basaltic and/or sedimentary bulk compositions in the amphibolite to eclogite facies undergo small degrees of partial melting at mantle depths, and where the resulting silica-rich melt passes upwards into mantle peridotite (Kesson et al., 1989; Kelemen et al., 1993). Reaction (2) is likely to occur where mantle-derived melts migrate upwards through peridotite along an adiabatic geothermal gradient (Kelemen et al., 1995a).

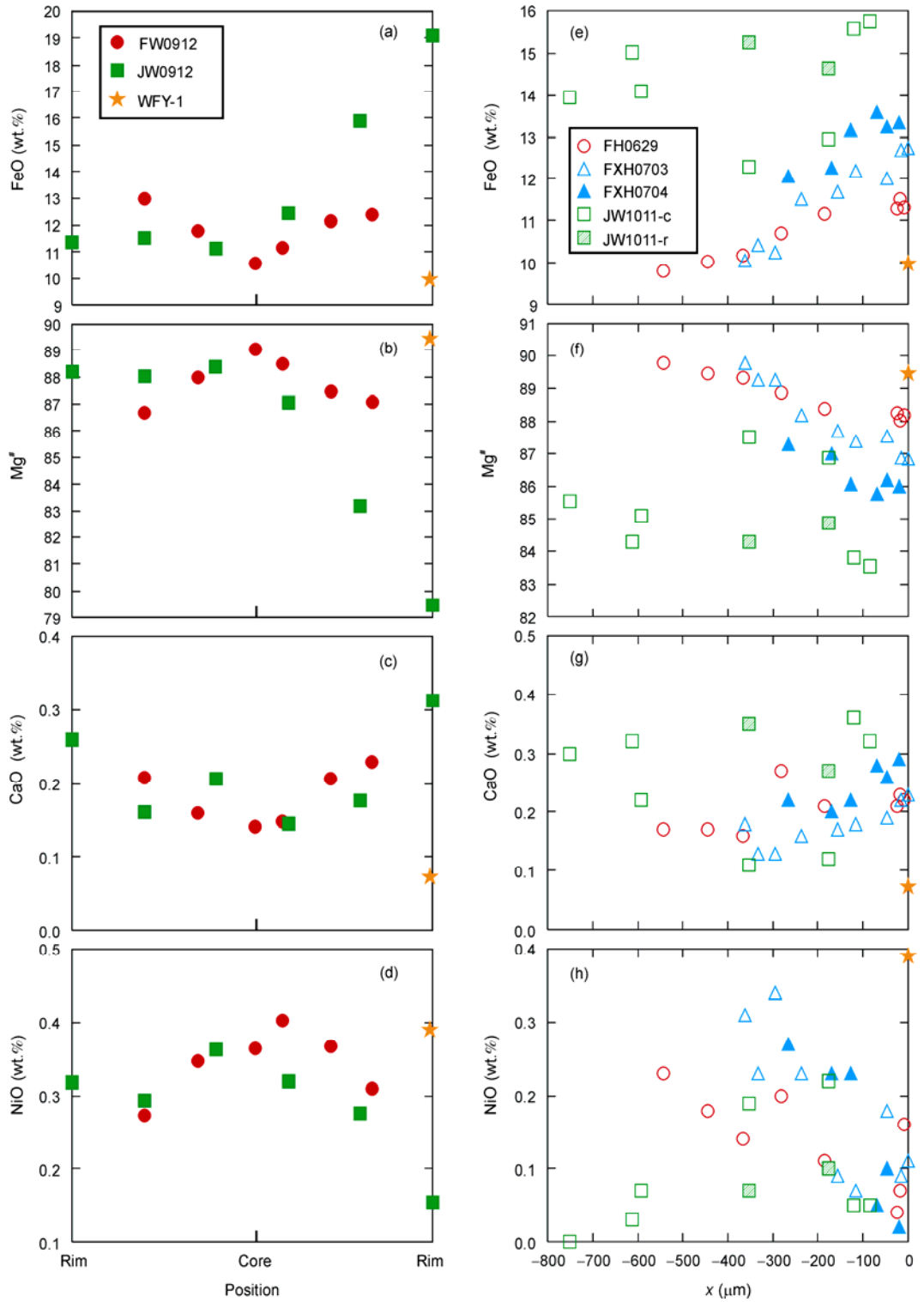

Figure 5 Plots of measured oxide abundance (in wt.%) in olivine as a function of analysis position and distance (x) in melt-peridotite layered experiments. The melt-peridotite interface is at x=0, and the crystal phase is at x<0.

Our experimental results show that the reactions between peridotite and either pyroxenite or a partial melt of pyroxenite (silica-rich melt) increase Opx proportions or SiO_2 contents in the peridotite. They also show that the reaction between a basaltic melt and peridotite tends to dissolve pyroxene and precipitate olivine. These results are consistent with previous experimental results (Yaxley et al., 1998; Rapp et al., 1999; Morgan et al., 2005; Lambart et al., 2009).

In the central-eastern NCC, we discovered different types

of peridotite xenoliths in the Mesozoic high-Mg diorites, including chromite-bearing dunite, dunite with orthopyroxenite veins, spinel harzburgite, and spinel lherzolite (Xu et al., 2003, 2008, 2010). Based on our experimental results, we conclude that the dunites with low-$Mg^{\#}$ olivines could result from basaltic melt-peridotite reactions, whereas orthopyroxenite veins in the dunites could have formed during a silica-rich melt-peridotite reaction. The former reaction results in the formation of depleted mantle, and the latter results in the transformation of depleted mantle to fertile lithospheric mantle. Our experimental results support the proposition that melt-peridotite reactions play an important role in transforming the nature of lithospheric mantle.

3.2 Origin of low-$Mg^{\#}$ dunite: Constraints from melt-peridotite reactions

Dunites are commonly observed in the mantle sections of ophiolite and peridotite massifs around the world (Boudier et al., 1985; Braun et al., 2002; Kubo, 2002). Some dunite bodies show evidence of magma-wall rock reactions in the upper mantle, and their formation would have changed the compositions of both the melt and the host peridotite (Kelemen, 1990; Kelemen et al., 1995b; Allan et al., 1996). The origins of dunites include: (1) as a residue formed by a high degree of partial melting of peridotite (Bernstein et al., 2007); (2) as a cumulate formed by the fractionation of olivine from a mafic melt (Zhang et al., 2005); and (3) as a replacement product formed during melt-peridotite reactions (Kelemen et al., 1998; Garrido et al., 2007).

The $Mg^{\#}$ of an olivine is usually used as a measure of the degree of partial melting and melt extraction in the mantle (Dick et al., 1984; Arai, 1994). Melting experiments indicate that a high $Mg^{\#}$ in the olivine implies a high degree of melting (Mysen et al., 1977). In our experiments, the $Mg^{\#}$'s of the olivines (83.6–89.3) in the dunite zone are lower than in the olivine of the starting material ($Mg^{\#}$=89.5). These lower values of $Mg^{\#}$ are similar to those in the dunite zone resulting from the alkali basalt-lherzolite reaction (Morgan et al., 2005), but they differ from those in the highly depleted peridotite where a high-$Mg^{\#}$ olivine was produced by a high degree of melting. As a result, we suggest that the reaction between basaltic magma and pyroxene-bearing peridotite could be responsible for the formation of low-$Mg^{\#}$ dunite. This conclusion is also supported by the trace element compositions of olivines from dunite xenoliths in western Shandong and the southern Taihang Mountains (Xu et al., 2008, 2010).

3.3 Variations of melt compositions: Implications for the origin of high-Mg adakitic rocks

Experimental studies have proved that partial melting of basaltic rocks will produce melts of low $Mg^{\#}$(<45) (Rapp, 1997). Reactions between melts and peridotite have been advocated to explain the generation of high-Mg ($Mg^{\#}$>45) tonalite-trondhjemite-granodiorite (TTG) and adakitic rocks (Kay, 1978; Yogodzinski et al., 1994, 2007; Kelemen, 1995; Gao et al., 2004; Xu et al., 2006; Wang et al., 2011; Castillo, 2012).

In our experiments, the reaction between Fuxin alkali basalt and peridotite results in an increase of SiO_2 and MgO and a decrease in FeO in the reacted melts. As the Feixian alkali basalt has more MgO but less FeO than the Fuxin alkali basalt, the reacted melt has a lower MgO and a higher FeO than the starting melt in the Feixian alkali basalt-peridotite reaction experiments. In the pyroxenite-peridotite reaction experiment (JW1011), the reacted melt has higher SiO_2 and MgO contents but lower Al_2O_3, FeO and CaO contents than the starting melts. The increases of the $Mg^{\#}$ in the reacted melts are similar to previous experimental results where the $Mg^{\#}$ increases in basaltic, slab-derived, or eclogite-derived melts (Rapp et al., 1999; Morgan et al., 2005; Yu et al., 2009; Wang et al., 2010; Mallik et al., 2012; Zhang et al., 2012).

Abundant dunite and harzbugite xenoliths are preserved in the Early Cretaceous high-$Mg^{\#}$ (63–67) diorites from western Shandong in the NCC. The vein or zoned Opx in dunite and some harzburgite xenoliths represents the product of adakitic metasomatism, and the high-$Mg^{\#}$ character of the diorites is thought to be the result of interaction between the adakitic melt and the peridotite (Xu et al., 2008). All of these have led us to the conclusion that melt-peridotite reactions could be responsible for the high-Mg signature of adakitic rocks.

4 Conclusions

We draw the following main conclusions from our HP-HT experiments:

(1) Reactions between basaltic melt and peridotite produce low-$Mg^{\#}$ dunites. Reactions between a pyroxenite-melt and peridotite produce low-$Mg^{\#}$ dunites at low pressures and orthopyroxenite layers at high pressures. Reactions between the partial melts (silica-rich) of pyroxenite and lherzolite also form layers of orthopyroxenite.

(2) The occurrence of different types of peridotite and pyroxenite xenoliths in western Shandong and the southern Taihang Mountains shows that the lithospheric mantle has undergone multiple periods of chemical change under the influence of a variety of melts.

(3) Melt-peridotite reactions could be responsible for transforming the nature of the lithospheric mantle, and for the high-Mg signature of adakitic rocks.

We thank all the staff members of State Key Laboratory of Geological Processes and Mineral Resources, China University of Geoscience, Wuhan, China, for their instruction and help in HP-HT experiments. Shu Guiming also kindly provided technical support during the electron microprobe

analysis. We are also grateful to the reviewers for their constructive comments. This study was financially supported by National Basic Research Program of China (Grant No. 2009CB825005) and National Natural Science Foundation of China (Grant Nos. 91014004 and 90814003).

Allan J F, Dick H J B. 1996. Cr-rich spinel as a tracer for melt migration and melt-wall rock interaction in the mantle: Hess Deep, Leg 147. In: Mével C, Gillis K M, eds. Proceedings of the Ocean Drilling Program, Scientific Results 147. College Station, TX: Ocean Drilling Program. 157–172

Arai S. 1994. Characterization of spinel peridotites by olivine-spinel compositional relationships: Review and interpretation. Chem Geol, 113: 191–204

Bernstein S, Kelemen P B, Hanghoj K. 2007. Consistent olivine $Mg^{\#}$ in cratonic mantle reflects Archean mantle melting to the exhaustion of orthopyroxene. Geology, 35: 459–462

Boudier F, Nicolas A. 1985. Harzburgite and lherzolite subtypes in ophiolitic and oceanic environments. Earth Planet Sci Lett, 76: 84–92

Braun M G, Kelemen P B. 2002. Dunite distribution in the Oman ophiolite: Implications for melt flux through porous dunite conduits. Geochem Geophys Geosyst, 3: 8603, doi: 10.1029/2001GC000289

Castillo P R. 2012. Adakite petrogenesis. Lithos, 134: 304–316

Chen L, Tao W, Zhao L, et al. 2008. Distinct lateral variation of lithospheric thickness in the northeastern North China Craton. Earth Planet Sci Lett, 267: 56–68

Deng J F, Su S G, Niu Y L, et al. 2007. A possible model for the lithospheric thinning of North China Craton: Evidence from the Yanshanian (Jura-Cretaceous) magmatism and tectonism. Lithos, 96: 22–35

Dick H J B, Bullen T. 1984. Chromian spinel as a petrogenetic indicator in abyssal and alpine-type peridotites and spatially associated lavas. Contrib Mineral Petrol, 86: 54–76

Fisk M R. 1986. Basalt-magma interactions with harzburgite and the formation of high magnesium andesites. Geophys Res Lett, 13: 467–470

Gao S, Rudnick R L, Yuan H L, et al. 2004. Recycling lower continental crust in the North China craton. Nature, 432: 892–897

Garrido C J, Bodinier J L, Dhuime B, et al. 2007. Origin of the island arc Moho transition zone via melt-rock reaction and its implications for intracrustal gifferentiation of island arcs: Evidence from the Jijal complex (Kohistan complex, northern Pakistan). Geology, 35: 683–686

Griffin W L, Zhang A D, O'Reilly S Y, et al. 1998. Phanerozoic evolution of the lithosphere beneath the Sino-Korean Craton. In: Flower M, Chung S L, Lo C H, et al., eds. Mantle Dynamics and Plate Interactions in East Asia. Am Geophys Union Geodyn Ser, 27: 107–126

Herrmann W, Berry R F. 2002. MINSQ—A least squares spreadsheet method for calculating mineral proportions from whole rock major element analyses. Geochem: Explor, Environ Anal, 2: 361–368

Kay R W. 1978. Aleutian magnesian andesites: Melts from subducted Pacific ocean crust. J Volcanol Geotherm Res, 4: 117–132

Kelemen P B, Hart S R, Bernstein S. 1998. Silica enrichment in the continental upper mantle via melt/rock reaction. Earth Planet Sci Lett, 164: 387–406

Kelemen P B, Joyce D B, Webster J D, et al. 1990. Reaction between ultramafic rock and fractionating basaltic magma (II): Experimental investigation of reaction between olivine tholeiite and harzburgite at 1150–1050°C and 5 kb. J Petrol, 31: 99–134

Kelemen P B, Shimizu N, Dunn T. 1993. Relative depletion of niobium in some arc magmas and the continental crust: Partitioning of K, Nb, La and Ce during melt/rock reaction in the upper mantle. Earth Planet Sci Lett, 120: 111–134

Kelemen P B, Whitehead J A, Aharonov E. 1995a. Experiments on flow focusing in soluble porous media, with applications to melt extraction from the mantle. J Geophys Res, 100: 475–496

Kelemen P B, Shimizu N, Salters V J M. 1995b. Extraction of mid-ocean-ridge basalt from the upwelling mantle by focused flow of melt in dunite channels. Nature, 375: 747–753

Kelemen P B. 1995. Genesis of high $Mg^{\#}$ andesites and the continental crust. Contrib Mineral Petrol, 120: 1–19

Kelemen P B. 1990. Reaction between ultramafic rock and fractionating basaltic magma (I): Phase relations, the origin of calc-alkaline magma series, and the formation of discordant dunite. J Petrol, 31: 51–98

Kesson S E, Ringwood A E. 1989. Slab-mantle interactions 2, the formation of diamonds. Chem Geol, 78: 97–118

Kubo K. 2002. Dunite formation processes in highly depleted peridotite: Case study of the Iwanaidake peridotite, Hokkaido, Japan. J Petrol, 43: 423–448

Lambart S, Laporte D, Schiano P. 2009. An experimental study of focused magma transport and basalt-peridotite interactions beneath mid-ocean ridges: Implications for the generation of primitive MORB compositions. Contrib Mineral Petrol, 157: 429–451

Mallik A, Dasgupta R. 2012. Reaction between MORB-eclogite derived melts and fertile peridotite and generation of ocean island basalts. Earth Planet Sci Lett, 329: 97–108

Menzies M A, Fan W M, Zhang M. 1993. Palaeozoic and Cenozoic lithoprobes and the loss of >120 km of Archaean lithosphere, Sino-Korean craton, China. In: Prichard H M, Alabaster T, Harris N B W, et al., eds. Magmatic Processes and Plate Tectonics. Geol Soc Spec Pub, 76: 71–81

Menzies M A, Xu Y G, Zhang H F, et al. 2007. Integration of geology, geophysics and geochemistry: A key to understanding the North China Craton. Lithos, 96: 1–21

Menzies M A, Xu Y G. 1998. Geodynamics of the North China Craton. In: Flower M, Chung S L, Lo C H, et al., eds. Mantle Dynamics and Plate Interactions in East Asia. Am Geophys Union Geodyn Ser, 27: 155–165

Morgan Z, Liang Y. 2005. An experimental study of the kinetics of lherzolite reactive dissolution with applications to melt channel formation. Contrib Mineral Petrol, 150: 369–385

Mysen B O, Kushiro I. 1977. Compositional variations of coexisting phases with degree of melting of peridotite in the upper mantle. Am Mineral, 62: 843–856

Pei F P, Xu W L, Wang Q H, et al. 2004. Mesozoic basalt and mineral chemistry of the mantle-derived xenocrysts in Feixian, western Shandong, China: Constrains on nature of Mesozoic lithospheric mantle (in Chinese). Geol J China U, 10: 88–97

Piccardo G B, Zanetti A, Müntener O. 2007. Melt/peridotite interaction in the Southern Lanzo peridotite: Field, textural and geochemical evidence. Lithos, 94: 181–209

Rapp R P, Shimizu N, Norman M D, et al. 1999. Reaction between slab-derived melts and peridotite in the mantle wedge: Experimental constraints at 3.8 GPa. Chem Geol, 160: 335–356

Rapp R P. 1997. Heterogeneous source regions for Archean granitoids. In: de Wit M J, Ashwal L D, eds. Greenstone Belts. Oxford: Oxford University Press. 35–37

Roeder P L, Emslie R F. 1970. Olivine-liquid equilibrium. Contrib Mineral Petrol, 29: 275–289

Sen C, Dunn T. 1994. Experimental modal metasomatism of a spinel lherzolite and the production of amphibole-bearing peridotite. Contrib Mineral Petrol, 119: 422–432

Shaw C S J, Dingwell D B. 2008. Experimental peridotite-melt reaction at one atmosphere: A textural and chemical study. Contrib Mineral Petrol, 155: 199–214

Wang C, Jin Z M, Gao S, et al. 2010. Eclogite-melt/peridotite reaction: Experimental constrains on the destruction mechanism of the North China Craton. Sci China Earth Sci, 53: 797–809

Wang D Y. 2002. Petrology and geochemistry of mafic-ultramafic inclusions in Mesozoic igneous rocks from western Shandong and western Liaoning: Implication for nature of Mesozoic lithospheric mantle (in Chinese). Doctoral Dissertation. Changchun: Jilin University

Wang Q, Li Z X, Chung S L, et al. 2011. Late Triassic high-Mg andesite/dacite suites from northern Hohxil, North Tibet: Geochronology, geochemical characteristics, petrogenetic processes and tectonic implications. Lithos, 126: 54–67

Wu F Y, Lin J Q, Wilde S A, et al. 2005. Nature and significance of the Early Cretaceous giant igneous event in eastern China. Earth Planet Sci Lett, 233: 103–119

Xu W L, Gao S, Wang Q H, et al. 2006. Mesozoic crustal thickening of the eastern North China Craton: Evidence from eclogite xenoliths and petrologic implications. Geology, 34: 721–724

Xu W L, Gao S, Yang D B, et al. 2009. Geochemistry of eclogite xenoliths in Mesozoic adakitic rocks from Xuzhou-Suzhou area in central China and their tectonic implications. Lithos, 107: 269–280

Xu W L, Hergt J M, Gao S, et al. 2008. Interaction of adakitic melt-peridotite: Implications for the high-Mg$^{\#}$ signature of Mesozoic adakitic rocks in the eastern North China Craton. Earth Planet Sci Lett, 265: 123–137

Xu W L, Wang D Y, Gao S, et al. 2003. Discovery of dunite and pyroxenite xenoliths in Mesozoic diorite at Jinling, western Shandong and its significance. Chin Sci Bull, 48: 1599–1604

Xu W L, Wang D Y, Wang Q H, et al. 2004. Metasomatism of silica-rich melts (liquids) in dunite xenoliths from western Shandong, China: Implication for Mesozoic lithospheric mantle thinning (in Chinese). Acta Geol Sin, 78: 72–80

Xu W L, Yang D B, Gao S, et al. 2010. Geochemistry of peridotite xenoliths in Early Cretaceous high-Mg$^{\#}$ diorites from the Central Orogenic Block of the North China Craton: The nature of Mesozoic lithospheric mantle and constraints on lithospheric thinning. Chem Geol, 270: 257–273

Xu Y G. 2001. Thermo-tectonic destruction of the Archaean lithospheric keel beneath the Sino-Korean Craton in China: Evidence, timing and mechanism. Phys Chem Earth (A), 26: 747–757

Yaxley G M, Green D H. 1998. Reactions between eclogite and peridotite: Mantle refertilisation by subduction of oceanic crust. Schweiz Mineral Petrogr Mitt, 78: 243–255

Yaxley G M. 2000. Experimental study of the phase and melting relations of homogeneous basalt + peridotite mixtures and implications for the petrogenesis of flood basalts. Contrib Mineral Petrol, 139: 326–338

Yogodzinski G M, Kelemen P B. 2007. Trace elements in clinopyroxenes from Aleutian xenoliths: Implications for primitive subduction magmatism in an island arc. Earth Planet Sci Lett, 256: 617–632

Yogodzinski G M, Volynets O N, Koloskov A V, et al. 1994. Magnesian andesites and the subduction component in a strongly calc-alkaline series at Piip Volcano, far western Aleutians. J Petrol, 35: 163–204

Yu Y, Xu W L, Liu X Y, et al. 2009. Hb-Grt-pyroxenite-peridotite reaction at 3.5 GPa and 1500°C: Preliminary experimental results and its geological implications (in Chinese). Prog Nat Sci, 19: 644–651

Zhang J F, Wang C, Wang Y F. 2012. Experimental constraints on the destruction mechanism of the North China Craton. Lithos, 149: 91–99

Zhang J, Zhang H F, Yin J F, et al. 2005. Are the peridotitic xenoliths entrained in Late Mesozoic intermediate-mafic intrusive complexes on the North China Craton: The direct samples of lithospheric mantle? (in Chinese) Acta Petrol Sin, 21: 1559–1568

Zheng C Q, Xu W L, Wang D Y. 1999. The petrology and mineral chemistry of the deep-seated xenoliths in Mesozoic basalt in Fuxin district from western Liaoning (in Chinese). Acta Petrol Sin, 15: 616–622